A Method for Extracting Phase Change Kinetics from Dilatation for Multistep Transformations: Austenitization of a Low Carbon Steel

R.C. DYKHUIZEN, C.V. ROBINO, and G.A. KNOROVSKY

This article describes the development of a method for determining phase change kinetics for multistep diffusion limited solid-state transformations from dilatation data. Since each step in a multistep reaction proceeds at a different rate, and the volume changes for the transformations are, in general, not equal, determination of the reaction kinetics from the dilatation data is not straightforward. Thus, a model is developed for the phase change process in which the transient dilatation is calculated based on the fractional extent of the various phases present. In this way, kinetic parameters are determined that allow the best match to the experimental data. However, both random and systematic experimental errors make reproduction of the experimental dilatation difficult. Therefore, a self-calibration process is developed that uses portions of the dilatation data to obtain the density variation of the various phases with temperature to help correct for experimental uncertainties. This procedure also enables the model to be used in situations where accurate property data are not available. The model and procedures are applied to the formation of austenite in a pearlite/ferrite low carbon steel where the pearlite and ferrite regions transform at different rates. A single kinetic parameter set allows reproduction of transformation transients of significantly different heating rates. These parameters can then be used to describe the austenitization for any time-temperature path. Excellent agreement between the model and experimental data is shown.

I. INTRODUCTION

THE formation of austenite is an important aspect of many metallurgical processing and fabricating schemes for steels. For example, hot working, heat treating, and welding all require or result in heating into the austenite plus ferrite or austenite phase fields. At the present time, there is widespread interest in modeling these processes as an aid in optimization and control of postprocess microstructure and properties. For these models to be applicable, they must describe the phase transformation kinetics associated with both the on-heating and on-cooling transformations, and these descriptions must be experimentally validated. In general, the formation of austenite in steels has received less attention than the decomposition of austenite, although there have been a number of experimental[1–6] and numerical studies[7–12] of the process. These studies have yielded significant insight into the transformation from both mechanistic and computational perspectives, but there are some limitations and difficulties in applying this insight to large scale process modeling.

As discussed by Gavard *et al.*[13] and Akbay *et al.*,[9] the formation of austenite differs from its decomposition in two principal ways. First, in the case of diffusion-limited on-cooling transformations, the driving force for the reaction increases with increasing undercooling below the equilibrium transformation temperature, while diffusion rates decrease with increasing undercooling. This balance between driving force and diffusion rates results in the classical *C*-curve kinetic behavior, in which the overall transformation rate experiences a maximum at intermediate undercoolings. In contrast, for the on-heating transformation, both the driving force and diffusion rates increase with temperature above the equilibrium transformation temperature, so that the rate of transformation continuously increases with temperature. Second, for the on-cooling reactions from homogeneous austenite, the kinetics can be fully described in terms of the composition and austenite grain size. Such a simplification is not possible for the formation of austenite, however, as a wide variety of starting microstructures are possible. Thus, the complexity of austenite formation implies that formulation of a general model for nonequilibrium conditions is likely to be exceedingly difficult.

Therefore, at the current time, it appears that separate models of austenite formation will be required for different initial microstructures. For the case of ferrite/pearlite initial microstructures, the formation of austenite is known to consist of two essentially distinct steps, which are associated with the decomposition of the two constituents. Hypoeutectoid carbon steels essentially consist of grains of pearlite surrounded by proeutectoid ferrite regions concentrated near the prior austenite grain boundaries. Upon heating, both regions transform to austenite. However, the transformation of the ferrite to austenite occurs at a significantly slower rate due to the fact that the carbon has to diffuse out of the former pearlite region into the low carbon ferrite regions. Thus, the process and, therefore, the kinetics of the transformation to austenite in the two regions are different.

In addition to the difficulties associated with modeling of austenite formation, experimental determination of the progress of the transformation during isothermal and non-

R.C. DYKHUIZEN, Principal Member of the Technical Staff, Thermal Sciences Department, and C.V. ROBINO, Principal Member of the Technical Staff, and G.A. KNOROVSKY, Senior Member of the Technical Staff, Materials Joining Department, are with Sandia National Laboratories, Albuquerque, NM 87185.

Manuscript submitted April 16, 1998.

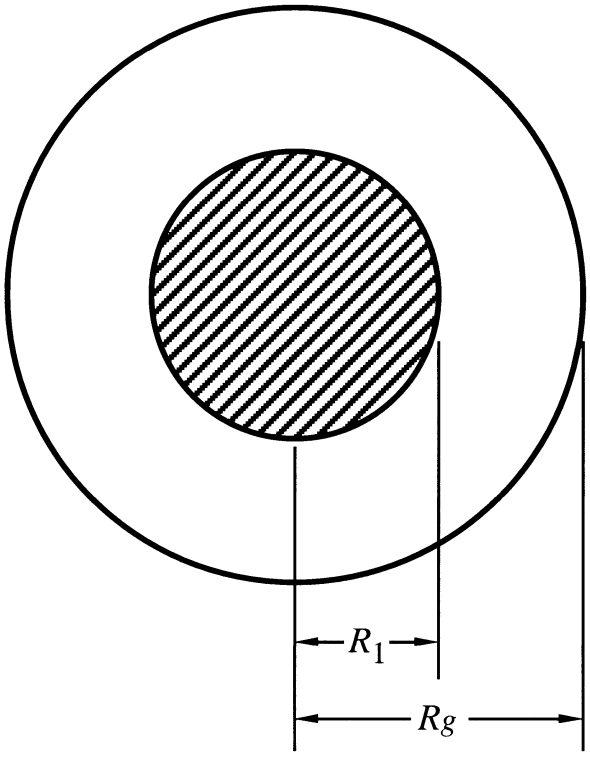

Fig. 1—Assumed initial grain geometry. R_g represents the prior austenite grain radius and R_1 is the initial pearlite colony radius.

isothermal heat treatments is also relatively complex, making calibration and validation of models problematic. Previous experimental studies of austenite formation have used either metallographic methods to determine the fraction of austenite after a specific thermal cycle or determinations of the lower and upper critical temperatures (such as by dilatometry) as means for validation of the models. In the former case, this approach is particularly suspect for nonisothermal heat treatments at high heating rates, since only a small number of points can be used to relate the time-temperature path to the time-fraction austenite path. In the latter case, only the beginning and end points of the transformation are used and the actual path of the transformation cannot be readily evaluated.

In the present work, the formation of austenite in a pearlitic low carbon steel was studied using a combined experimental and numerical approach. The progress of the austenitization reaction over a range of heating rates was tracked experimentally through dilatometric measurements. In the conventional approach, the fraction transformed is inferred from such records by assuming a simple linear relationship between the fraction transformed and dilatation measured. For the case of continuous heating or cooling, the fraction transformed is obtained from extrapolated dilatation *vs* temperature curves for the parent and product constituents. In either case, a transformation model is then applied to fit the inferred fraction transformed *vs* time/temperature path.

Recent work by Onink *et al.*[14] on the on-cooling decomposition of austenite has demonstrated that such an approach can introduce significant errors. These errors essentially result from the fact that three phases are involved in the transformation, and the dilatation (lattice parameter) of the austenite is strongly dependent on its carbon content as well as temperature. Thus, the fraction transformed is not a linear function of the relative length change and cannot be directly inferred from a dilatation *vs* time/temperature record. In order to avoid this difficulty in the current work, the dilatation record from constant heating rate experiments was fit directly using temperature and composition-dependent densities coupled with a transformation model similar to that recently described by Oddy *et al.*[15] From this direct fit, the fraction austenite versus the time/temperature path is derived. The model treats the formation of austenite from the pearlite/ferrite mixture as a two-part process, one describing the transformation of pearlite and one describing the growth of austenite into the proeutectoid ferrite.

Finally, random and systematic experimental errors make reproduction of the experimental dilatation difficult. Therefore, a self-calibration process is developed that uses the dilatation data to also obtain the density variation of the various phases with temperature. This procedure not only helps to correct experimental uncertainties, but also enables the model to be used in situations where accurate property data are not available.

Application of the self-calibration method requires that a kinetic model be formulated first to describe the features of the transformation. This model may be of arbitrary complexity and may include many individual transformation steps.

The second step is the self-calibration step. Here, models are written to express the phase densities as a function of temperature and composition. The model parameters are then adjusted so that the dilatation curve is matched in regions removed from the region where the transformations take place. In this way, the effects of experimental errors and inaccurate phase density models are minimized. The equations developed in the first two steps are then combined to enable calculation of the change in the sample volume as the transformation proceeds.

The final step is to use a fitting procedure to obtain values for a finite set of kinetic parameters that yield the best fit to the dilatation data. For this step, it is preferable to use a variety of transients (*e.g.*, various heating rates) in determining the kinetic parameters. Correct models and accurate experimental data will result in good agreement between the predictions and experiments with a minimum of adjustable fitting parameters. In this article, the self-calibration method is described *via* an example application—the austenitization of a low carbon steel. Since the volume changes, as well as the rates of the two constituent reactions, are different, extraction of the reaction kinetics from the dilatation data is difficult. Thus, the transformation kinetics of each region are modeled separately. This requires inclusion of two reaction rates into the model and, of equal importance, the different volume changes associated with each part of the transformation.

II. MODEL DEVELOPMENT

A. *Initial Conditions and Geometry*

To formulate the kinetic model, the first step is to establish a typical geometry. The reaction rates are known to be a function of the distances over which the carbon must diffuse, so the physical grain size is an important parameter.

Figure 1 shows the assumed simplistic spherical geometry of a typical grain. Each heat will be represented by a single representative prior austenite grain size, R_g, which is a required input to the model. The grain size of a particular heat can be estimated from micrographs.

The kinetic model also requires input of the initial pearlite volume fraction, which can also be determined from micrographs by quantitative image analysis. A third required input is the alloy density, which is also easily measured. The model output (reaction kinetics), however, is not dependent upon this input. This insensitivity is due to the self-calibration feature presented later in this article. Finally, the average carbon content of the alloy and the alloy eutectoid temperature are required inputs. From the pearlite volume fraction, F_p, and the spherical approximation, the average size of the pearlite region within a grain, R_1, can be expressed as

$$R_1 = R_g(F_p)^{1/3} \quad [1]$$

B. *Austenitization Kinetics*

Next, physical models are postulated for the phase change of the various regions to austenite after the eutectoid temperature is exceeded. The eutectoid temperature can be experimentally determined from a slow (<1 degree centigrade per second) dilatation experiment or by compositional critical temperature correlations available in the literature.[16] It is assumed that the transformation from pearlite to austenite follows Avrami kinetics[18] and can be modeled as an additive reaction.[18] These assumptions result in the following differential equation for the reaction extent (Oddy *et al.*,[15] and Jacot *et al.*[19]):

$$\frac{dA}{dt} = (A_{\max}(T) - A)nK(T)\theta^{(n-1)}$$

where

$$\theta = \left[\frac{-\ln\left(\frac{A_{\max}(T) - A}{A_{\max}(T)}\right)}{K(T)}\right]^{1/n} \quad [2]$$

and

$$K(T) = \exp\left(\alpha - \frac{\beta}{T}\right)$$

In this kinetic model, A is the fraction of pearlite transformed to austenite and $A_{\max}(T)$ represents the maximum (value of the extent of transformation) as a function of the temperature (T). For the transformation of the pearlite, this is simply a unit step function, equal to 1 above the eutectoid temperature. The term n is the order of the reaction and assumed equal to 3 based on data presented by Speich and Szirmae.[3] The term θ is a fictitious time and is set equal to the time required to obtain the current extent of reaction at the current temperature. This parameter assures reproduction of the isothermal time-temperature-transformation (TTT) diagrams for reactions of order n and is the basis of the additivity assumption.[18] The term $K(T)$ is a temperature-dependent rate parameter. In principal, it could be determined from a detailed TTT diagram for eutectoid pearlite. However, we assume the functional form given in Eq. [2] and determine two parameters, α and β, by fitting experimental data. This eliminates the need for a detailed TTT diagram for the specific alloy. The functional form of $K(T)$ is consistent with isothermal austenitization experiments reported by Speich and Szirmae.[3]

A separate kinetic model is used for the ferrite region that surrounds the pearlite. The diffusion-limited model for the austenitization of ferrite is very similar to others (Oddy *et al.*,[15] Judd and Paxton,[5] and Molinder[4]). The differences between the current model and the earlier models will be discussed after our model is presented. It is assumed here that the conversion of the ferrite region to austenite does not initiate until the pearlite region is one-tenth transformed to austenite. The ferrite cannot transform near the eutectoid temperature until carbon is available from the pearlite region. Hence, it is not reasonable to allow diffusion of carbon out of the pearlite region until it is freed from the cementite. In fact, allowing the transformation of ferrite to initiate simultaneously with the transformation of the pearlite resulted in poor fits to the dilatation data. The choice of a particular value of the extent of reaction is not important, for it is found experimentally that the transformation of pearlite to austenite proceeds very rapidly between 10 and 90 pct completion in the current experiments and simulations.

Thus, the transformation of the ferrite region to austenite is delayed and proceeds at a significantly slower rate. It is assumed that this transformation is limited by the diffusion of carbon from the former pearlite region outward. The following approximate equation was developed to describe the movement of the transformation front:

$$\frac{dr}{dt} = \left(\frac{\gamma D(T)\frac{\Delta c}{\Delta x}}{c_i(T) - c_{fo}}\right)\left(\frac{R_{\max}(T) - r}{R_g - R_1}\right) \quad [3]$$

In Eq. [3], r represents the radial location within the grain that marks the boundary between the untransformed ferrite (at larger radii) and the austenite. The range of this variable is R_1, to $R_{\max}(T)$. The right-most term in parentheses in Eq. [3] is included to limit the growth of the phase boundary to less than $R_{\max}(T)$. This last term is of order unity for most of the transient, so its functional form does not greatly influence the predictions; however, it is conceptually similar to the impingement term in the Avrami equation.

The functional form of $R_{\max}(T)$ is easily determined. Prior to transformation of 10 pct of the pearlite to austenite, $R_{\max}(T)$ is set equal to R_1, so the phase boundary does not move. Above the upper critical temperature, $R_{\max}(T)$ is set to the grain boundary radius, R_g. Between these two limits, $R_{\max}(T)$ is set to the value that yields the appropriate austenite/ferrite two-phase mixture at equilibrium. This value is obtained from phase diagram lever rule estimates for the particular steel being evaluated.

The denominator of the first term on the right-hand side of Eq. [3], $(c_i(T) - c_{fo})$, represents the carbon concentration change required to advance the boundary. The term c_{fo} is the initial carbon concentration in the ferrite, and $c_i(T)$ is the austenite carbon concentration at the interface, $c_i(T)$ is determined from the A_{e3} line for the particular steel composition. This line must be consistent with the eutectoid

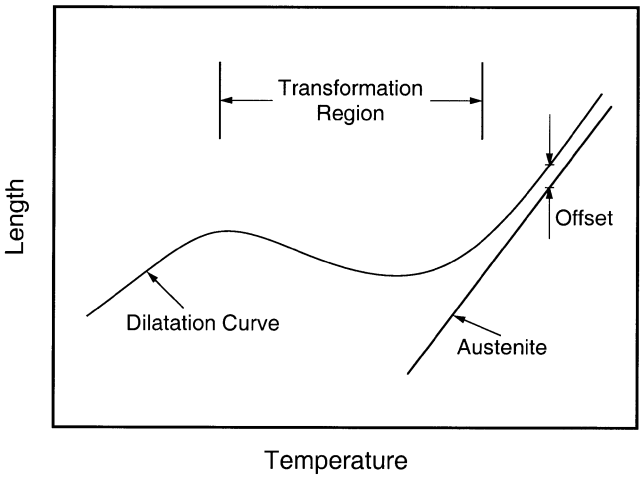

Fig. 2—Schematic experimental dilatation curve (above) compared to one calculated based on the austenite density variation with temperature. An offset, as depicted, will yield significant modeling errors.

carbon concentration calculated in Section C. The following form for the A_{e3} line is used, with the parameter g chosen so that the eutectoid concentration is obtained at the eutectoid temperature:

$$c_i(T) = ((T_1 - T)g)^{1/2} \quad [4]$$

where T_1 is the intercept of the A_{e3} line at 0 wt pct C (888 °C for the current steel). We have found the form of Eq. [4] to be a reasonable fit to the upper critical line for low carbon alloys, and it is consistent with the empirical relationships given by Andrews.[16]

If $c_i(T)$ reduces to the initial carbon concentration in the ferrite, the phase boundary is predicted to grow with infinite speed. This is because the reaction rate is no longer controlled by carbon diffusion as assumed. Depending upon the temperature ramp rate, the transformation is typically predicted to be essentially complete prior to this occurring, so this difficulty is avoided in practice. However, the computer representation of Eq. [3] limits $c_i(T)$ to one-tenth of the eutectoid carbon concentration to unequivocally avoid this problem.

The concentration gradient from Eq. [3] is approximated by

$$\frac{\Delta c}{\Delta x} = \frac{c_i(T) - c_e}{2(r - R_1)} \quad [5]$$

where $c_i(T)$ is the carbon concentration at the ferrite/austenite interface and c_e is the intital concentration in the pearlite. The effective distance over which this concentration difference is applied is assumed to be represented by $2(r - R_1)$. This form assumes that the ''wave front'' of reduced carbon content travels the same distance into the pearlite that the wave front of increased carbon content travels into the ferrite. The term $D(T)$ is the diffusion coefficient of carbon in austenite.[17] The variation of the diffusion coefficient with carbon content and the effects of other elements, such as manganese, are not considered. Finally, γ is introduced as a fitting constant, and it is expected that it will be near unity. In essence, this fitting constant compensates for differences between the assumed and actual (nonspherical) ferrite geometry, as well as the simplifications regarding carbon diffusion in austenite.

From the radial location of the austenite/ferrite interface, the fraction of the ferrite region that has reacted can be determined:

$$B = \frac{r^3 - R_1^3}{R_g^3 - R_1^3} \quad [6]$$

The model described by Eqs. [1] through [6] is similar to that developed by others. Judd and Paxton[5] and Molinder[4] used similar expressions for the diffusional decomposition of the ferrite. However, both studies limited the model to temperatures below the A_{e3} line. This limit eliminated the problems associated with predicting infinite interface velocities when the interfacial carbon concentration falls below the carbon concentration in the ferrite.

Oddy *et al.*[15] proposed a similar, but more complex, model to determine the carbon diffusion into the ferrite, which included two fitting constants. These fitting constants were expected to be similar in magnitude and near unity, yet they were determined to be an order of magnitude apart. In the current work, the more complex model described by Oddy *et al.* was avoided and the simpler Eq. [3] was developed. Since the generalized geometry of Figure 1 is simplistic (but essentially identical to that used by Oddy *et al.*), it is believed that a more complex model is not justified.

C. *Self-Calibration of the Phase Densities*

The experimental dilatation data are used to determine both the reaction extent and the densities of the various phases as a function of temperature. Density variations may also be determined from the literature; however, by using the experimental dilatation data directly, the following advantages are realized.

(1) The need for an accurate chemical analysis is reduced.
(2) The need for density data applicable to the exact alloy used is eliminated.
(3) The effects of systematic and random errors in the experiment are minimized.

The use of self-calibrated densities allows the fitting process to concentrate on the important portion of the dilatation curve. This advantage can be best explained by considering a case where self-calibration is not applied. Figure 2 shows a schematic overlay of a typical curve for austenite density along with a measured dilatation curve. Due to a variety of factors, such as uncertainty in the dilatometer output, the two curves will not generally overlay exactly in the fully austenitic region. The case depicted considers the situation where the measured dilatation curve is above, but parallel to, the curve based on the tabulated austenite density. The best fit of a kinetic model will be obtained by choosing fitting parameters that significantly delay the transformation to austenite and even prevent the completion of the transformation. In effect, this would raise the calculated dilatation curve above the austenite curve and yield a better ''fit'' to the data. However, experience would indicate that the reaction is complete once the two curves are parallel and the offset is simply a manifestation of experimental error or an error in the tabulated austenite density.

By using the self-calibration method, the phase densities are adjusted so that the dilatation curve overlays those for

the constituents away from the reaction region. In the typical case, the dilatation curve is first smoothed to reduce noise and adjusted so that the initial dilatation at a standard state is zero. Since both ferrite and cementite exist in the initial condition, it is impossible to determine both phase densities from a single measurement. One approach would be to use tabulated (or reference) densities for one of the two phases and then adjust the other phase density so that the measured value is reproduced. In the current application, the reference densities for both the cementite and ferrite were adjusted with a common multiplier so that the measured initial density of the sample was reproduced.

The following describes in detail how the adjustments are made. The functional forms for the ferrite and cementite densities were obtained from the lattice parameters given by Onink *et al.*[14] Measured values for the average carbon content $\bar{c}$ and the material density ρ_o are inputs to the following equation set. From these, the density multiplier ω_o and the initial volume fraction of the cementite F_{co} are obtained by solution of the following equation set:

$$\begin{aligned} \rho_o \bar{c} &= \omega_o (F_{co}\rho_{co}c_{co} + (1 - F_{co})\rho_{fo}c_{fo}) \\ \rho_o &= \omega_o (F_{co}\rho_{co} + (1 - F_{co})\rho_{fo}) \end{aligned} \quad [7]$$

In Eq. [7], the ferrite fraction includes the ferrite in both the pearlite and proeutectoid ferrite constituents. The pearlite phase density is then obtained from the following equation:

$$\rho_o = F_{po}\rho_{po} + (1 - F_{po})\rho_{fo} \quad [8]$$

The initial cementite volume fraction within the pearlite, F^p_{co}, can be determined from either of the following equations:

$$\begin{aligned} \rho_{po} &= F^p_{co}\rho_{co}\ (1 - F^p_{co})\rho_{fo} \\ F_{co} &= F_{po}F^p_{co} \end{aligned} \quad [9]$$

The initial pearlite carbon concentration, c_{po}, can be determined from the following equation:

$$\rho_{po}c_{po} = F^p_{co}\rho_{co}c_{co} + (1 - F^p_{co})\rho_{fo}c_{fo} \quad [10]$$

The initial pearlite carbon concentration is assumed to be equal to the eutectoid carbon concentration. This assumption eliminates the need for a phase diagram for the particular alloy and does not require a chemical analysis of the alloy (although measurements of the average carbon content and pearlite fraction of the alloy are required). Using this eutectoid carbon concentration, the eutectoid temperature, and T_1, the A_{e3} line is constructed (Eq. [4]).

Next, a linear fit to the dilatation data below the reaction region (from 50 °C below the eutectoid temperature to the eutectoid temperature) is obtained. This fit is then evaluated to obtain an experimental value for the dilatation at the eutectoid temperature. Use of the fit minimizes the effect of experimental noise. The density of the original phase mixture at the eutectoid temperature is determined from the following relation:

$$\rho_e = \rho_o \left(\frac{L_o}{L_o + \Delta L(T_e)} \right)^3 \quad [11]$$

where L_o is the sample length (or diameter) at the reference temperature and $\Delta L(T_e)$ is the measured change in the length (or diameter) at the eutectoid temperature.

As noted previously, it is impossible to extract the thermal expansion of both phases with this one measurement. Therefore, a new common multiplier is introduced. This adjusts the cementite and ferrite densities at the eutectoid temperature to enable the model to reproduce the measured dilatation at this temperature.

The following equation is used to determine both the volume fraction of cementite at the eutectoid temperature and the eutectoid multiplier.

$$\begin{aligned} \rho_e \bar{c} &= \omega_e (F_{ce}\rho_{ce}c_{co} + (1 - F_{ce})\rho_{fe}c_{fe}) \\ \rho_e &= \omega_e (F_{ce}\rho_{ce} + (1 - F_{ce})\rho_{fe}) \end{aligned} \quad [12]$$

It is assumed in Eq. [12] that the carbon concentrations of the two phases do not change as the temperature of the sample is raised to the eutectoid temperature. Use of the two density multipliers (ω_o, ω_e) compensates for any errors in the dilatometry. In the current work, all adjustments were less than 1 pct. Linear extrapolation of the line fit through the two multipliers allows the model to calculate the densities for these two phases above the eutectoid temperature.

The high-temperature dilatation data are used to determine the density of the austenite formed as a function of temperature. Here a linear fit of all the data within 150 °C of 1000 °C is used. From this fit, both the high-temperature density and the thermal expansion coefficient can be determined. The high-temperature density of the austenite is determined from the measured dilatation at 1000 °C:

$$\rho_a(1000) = \rho_o \left(\frac{L_o}{L_o + \Delta L_a(1000)} \right)^3 \quad [13]$$

A low-temperature density for austenite is then determined by extrapolating the dilatation data to T_o using the slope determined at 1000 °C:

$$\begin{aligned} \Delta L_a(T_o) &= \Delta L_a(1000) + (T_o - 1000)\,\frac{\Delta(\Delta L_a)}{\Delta T} \\ \rho_{ao} &= \rho_o \left(\frac{L_o}{L_o + \Delta L_a(T_o)} \right)^3 \end{aligned} \quad [14]$$

The austenite density is assumed linear with temperature between the two values determined previously:

$$\rho_a(T, \bar{c}) = \rho_{ao} + \left(\frac{T - T_o}{1000 - T_o} \right)(\rho_a(1000) - \rho_o) \quad [15]$$

Using the preceding procedure, the model predictions are constrained to reproduce both the high- and low-temperature portions of the dilatation curve.

By adjusting the densities of the various phases, we can account for systematic errors in our measurements of dilatation as a function of temperature (or time). Further, by fitting our predictions to the entire experimental data set, the effects of random errors are minimized, since, by definition, random errors will be both positive and negative. If an analogy between experimental errors and a.c. electrical circuits can be drawn, the systematic errors can be viewed as a d.c. offset and the random errors can be viewed as the high frequency portion of the signal. Our procedure helps minimize the effects of very high and low frequency errors in the signal, but intermediate frequencies cannot be

Table I. Alloy Composition

Element	Concentration (Wt Pct)
C	0.29
Mn	0.82
Si	0.17
Ni	0.07
Cr	0.10
Mo	0.02
Cu	0.16
Al	0.030
N	0.0081
P	0.012
S	0.024
Fe	balance

counteracted. Thus, good experimental data, as always, are desired.

It is still left to determine how the austenite density changes with carbon content. This is important since the average carbon content of the austenite changes during the dilatation transient. The austenite carbon content is initially equal to the eutectoid value and then reduces as more of the ferrite region is transformed. Equation [15] only determines the density of the austenite at the average carbon content and must be modified to calculate the density of austenite for other carbon concentrations. This is done by using the following equation:

$$\rho_a(T, \bar{c}) = \rho_a(T, \bar{c}) \frac{\rho_{\text{ref}}(T, c_a)}{\rho_{\text{ref}}(T, \bar{c})} \quad [16]$$

where ρ_{ref} is the density of austenite as a function of temperature and carbon content that is obtained from a standard reference. The lattice parameters given by Onink *et al.*[14] are used to obtain these functional forms.

In essence, the self-calibration method allows the fitting process to concentrate on obtaining parameters that will describe the kinetics of the reaction, since use of the densities derived from the dilatation data will guarantee appropriate fits away from this region. In this sense, the procedure is similar to what is conventionally done to determine phase extent from dilatation curves for single-step transformations.

D. *Dilatation Calculation*

In this section, the calculation of the sample dilatation from the reaction extent is described. This is done by determination of the mass fractions of each phase and the individual phase densities as a function of temperature and carbon content.

The mass fractions of the three phases during the transient are determined from integration of Eqs. [2] and [3]. The mass fraction of the austenite (M_a) formed is found from the following sum:

$$M_a = AM_{po} + (1 - M_{po})B \quad [17]$$
$$M_{po} = \frac{F_{po}\rho_{po}}{\rho}$$

where A and B are defined in Eqs. [2] and [6], respectively, and M_{po} is the initial mass fraction of the pearlite. The first term in Eq. [17] represents the austenite formed from the pearlite, and the second term represents the austenite formed from the proeutectoid ferrite regions. The mass of cementite is determined from the following equation, which assumes that the cementite and the ferrite are consumed proportionally as the pearlite transforms to austenite:

$$M_c = (1 - A)M_{co} \quad [18]$$

Currently, the model does not preferentially transform the ferrite within the pearlite, as was experimentally observed by Speich and Szirmae.[3] The mass fraction of ferrite can be obtained similarly or simply by the fact that the remaining mass fraction must be ferrite.

The initial ferrite carbon concentration and the initial pearlite carbon concentration are used to calculate the densities of the unreacted species. However, it is left to determine the changing austenite carbon content. Since the lattice parameter of austenite is a linear function of the carbon content, it is a reasonable approximation to use the current average carbon content to calculate a single transient austenite density. The average carbon concentration of the austenite is determined from the average composition of the phases that have transformed.

$$c_a = \frac{M_{po}Ac_e + (1 - M_{po})Bc_{fo}}{M_a} \quad [19]$$

The dilatation is then calculated from the following:

$$\frac{V(T)}{V_o} = \frac{M_a\rho_a + M_c\rho_c + M_f\rho_f}{\rho_o} \quad [20]$$
$$\frac{\Delta L}{L_o} = \left(\frac{V(T)}{V_o}\right)^{1/3} - 1$$

Completion of the model requires determination of the three kinetic parameters (α, β, and γ). This is done by finding the best root-mean-square fit to the smoothed experimental data obtained at three different heating rates. The Simplex method (Press *et al.*[20]) is used to obtain this fit.

III. EXPERIMENTAL PROCEDURES

The composition of the steel used in this investigation is shown in Table I and meets the requirements for SAE/AISI 1026 plain carbon steel. The starting microstructure for this steel is shown in Figure 3 and consists of a ferrite/pearlite aggregate. Dilatometry was conducted on a DSI Gleeble 1500 thermomechanical simulator. Diametral dilatation was measured on 6.35-mm-diameter samples using a high resolution dilatometer at the location of a Cr-Al thermocouple percussion welded to the sample. The dilatometer was calibrated for each of the heating rates by using pure nickel samples of the same geometry. All tests were conducted in a vacuum purged enclosed chamber under flowing high purity argon with computer data acquisition at high sampling rates. The tests were conducted using programmed linear heating rates ranging from 50 to 300 °C/s. Samples for metallography were prepared using standard polishing techniques and were etched using 2 pct nital. Determinations of the relative fractions of individual microstructural constituents were conducted using quantitative image analysis software.

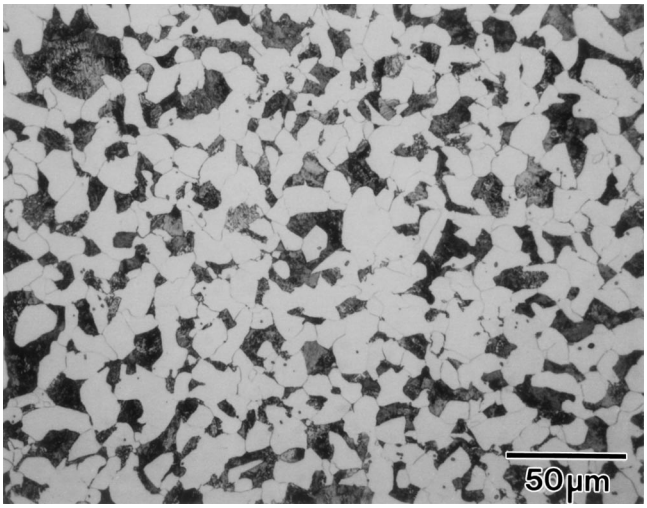

Fig. 3—Initial microstructure of 1026 alloy.

IV. RESULTS

A. *Model Estimates*

The procedure described in Section II was used to determine the reaction kinetics of the 1026 alloy. For these determinations, temperature ramp rates of 50 °C/s, 100 °C/s, and 200 °C/s were fitted with the model. Inputs to the model were the experimentally determined room-temperature density, 7.84 g/cm^3; the metallographically determined pearlite volume fraction, 0.333; the metallographically determined grain size, 24 μm; an estimate[16] of the eutectoid temperature, 720 °C; and the diffusion coefficient of carbon in austenite.[17] Each dilatation data set was self-calibrated so that errors in the individual experiments could be separately accounted for, but a single set of kinetic parameters was used to fit all three experimental data sets simultaneously. Figure 4 shows comparisons between the experimental and best model fits for dilatation *vs* time (Figure 4(a)) and *vs* temperature (Figure 4(b)). In general, the model captures the detailed characteristics of the experimental data. For example, the 200 °C/s heating rate shows two local minima in the dilatation *vs* time curve, and this behavior is reflected in the model fits (the reasons for the local minima are discussed subsequently). Further, comparison of the model prediction with replicated experimental determinations indicated that the model prediction typically falls within the experimental variance.

The values obtained for the pearlite decomposition in the 1026 alloy were approximately $\alpha = 201$ and $\beta = 200{,}000$ K. Using Eq. [2] to obtain a time constant for the pearlite transformation, these parameters result in faster time constants than those reported by Oddy *et al.*[15] (based on the data presented by Speich and Szirmae[3]), especially at the low values of superheat. It was found in this study that use of the logarithmic functional form used by Oddy *et al.* for the pearlite reaction time constant, instead of the Arrhenius form (Eq. [2]), could not reproduce all of the temperature rate transients with the same parameter values. The diffusion parameter (γ) was found to be 2.23, which is of order unity, as expected. Closer agreement to this cannot be expected since the geometry is much more complex (Figure 3) than assumed by Figure 1, and the effects of ternary elements on carbon diffusion in austenite are not considered.

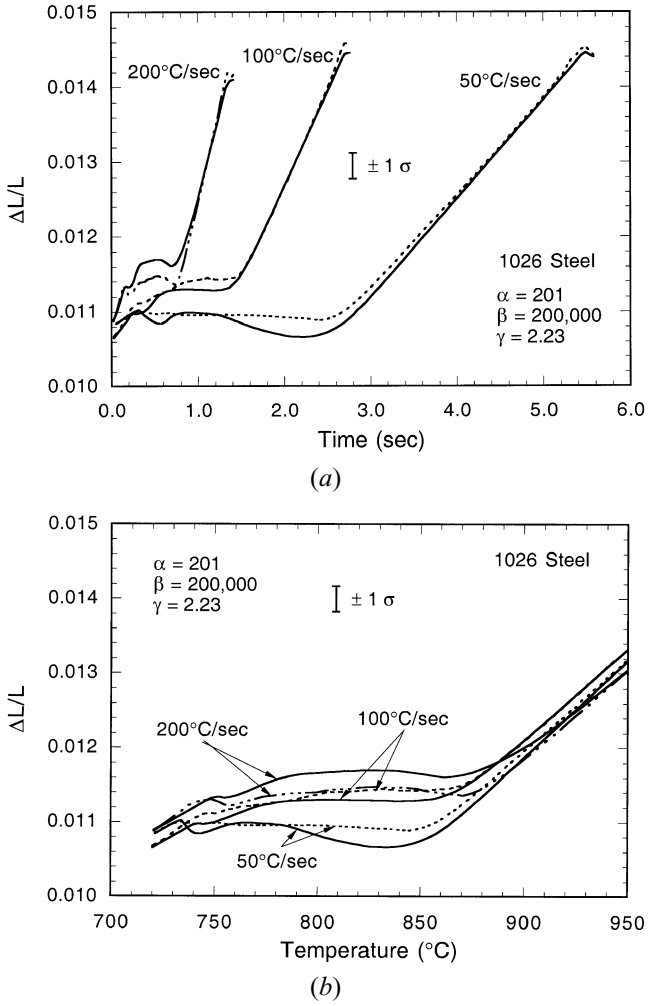

Fig. 4—Comparison of experimental dilatation data (dashed) to prediction (solid) for three different heating rates: (*a*) time dependence and (*b*) temperature dependence. Error bar is $\pm 1\ \sigma$ and represents variance of dilatometer data at 700 °C for three determinations at each of three heating rates.

Figure 5 shows the individual contributions of the pearlite and ferrite to the total fraction austenite as a function of temperature for the 100 °C/s heating rate. As might be expected, formation of austenite from the pearlite occurs at a significantly higher rate than the formation of austenite from ferrite. This difference is a consequence of the very short carbon diffusion distance (on the order of 1 μm) in the pearlite and is responsible for the initial local minima in the dilatation *vs* time or temperature records (Figures 4(a) and (b), respectively). The current model assumes that the cementite and ferrite within the pearlite are consumed proportionally, so that neither phase remains when the pearlite is transformed to austenite. Speich and Szirmae[3] and others[2,6] have shown that cementite (and/or carbon concentration gradients) can remain in austenite formed from pearlite. This effect, however, cannot be easily captured in the Avrami description (or other descriptions) of the pearlite decomposition. However, it is believed that for the heat-

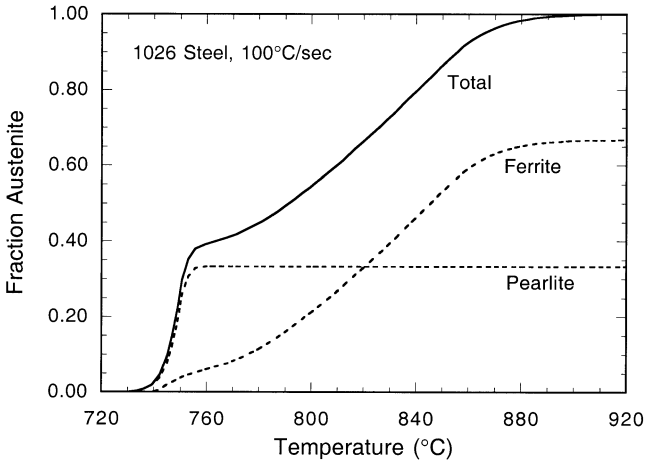

Fig. 5—Fraction austenite as a function of temperature for the 100 °C/s heating rate. The relative contributions from the pearlite and ferrite constituents are also shown.

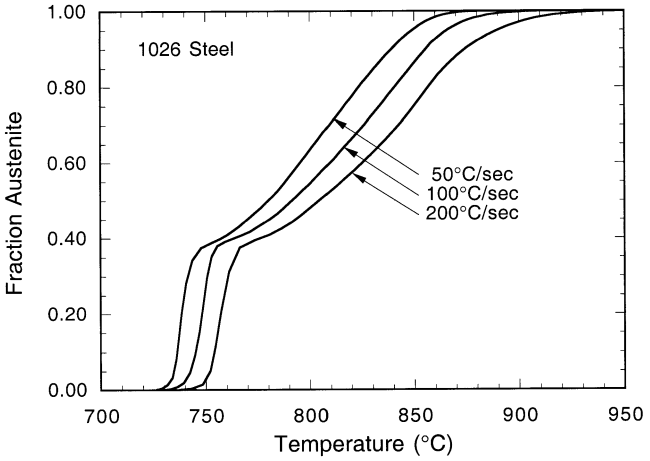

Fig. 6—Austenite fraction as a function of temperature for the heating rates of 50, 100, and 200 °C/s.

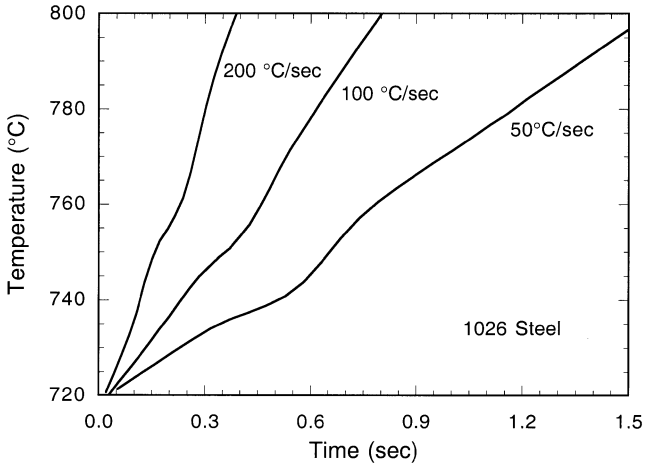

Fig. 7—Actual thermal cycles for the three heating rates used in the model fits.

ing rates and relatively fine pearlite in the current work, this is a second-order effect and does not dramatically influence the overall kinetic determinations.

Figure 6 shows the fraction austenite as a function of temperature for the three heating rates. As might be expected, the reaction is generally shifted to higher temperatures for the higher heating rates. The overall shape of the curves, while being very similar, does not allow for superposition (as would occur for a strictly additive reaction[18]). The main difference is in the slopes of the curves after the transition from pearlite dissolution to proeutectoid ferrite dissolution. The faster heating rates delay the transformation to higher temperatures (*i.e.*, reduce the slope at a given fraction austenite). There are also slight differences between the shapes of the curves during the pearlite decomposition, which are just evident in Figure 6. These differences are due to deviations from the programmed linear heating rate and result from thermal arrests associated with the latent heat of the transformation. The actual thermal cycle experienced by the sample for several heating rates is shown in Figure 7. In addition to the lag associated with the latent heat, there can also be a brief overshoot relative to the programmed temperature ramp due to the temperature control algorithm overcompensating for the arrest. Both of these deviations contribute to the complexity of the dilation curves. Nevertheless, it is important to note that the actual temperature cycle is used in the fitting routine, so that the effects of these deviations on the determined kinetics are accounted for. In an effort to evaluate the effects of the latent heat more fully, however, experiments in which the Gleeble was modified to operate in a controlled-power mode, rather than the conventional controlled-temperature mode, were conducted. The results of these experiments are summarized subsequently, while a more detailed description of the experiments and Gleeble modifications are given elsewhere.[21] In the controlled-power mode tests, constant power levels, which produced heating rates similar to the controlled-temperature cycle tests, were used. For these experiments, the Gleeble does not respond to the transformation by the application of additional power, so the temperature cycles show pronounced thermal arrests near the lower critical temperature (and hence lower transformation rates for a given heating rate). An example of these arrests is shown in Figure 8 for a 100 °C/s heating rate.

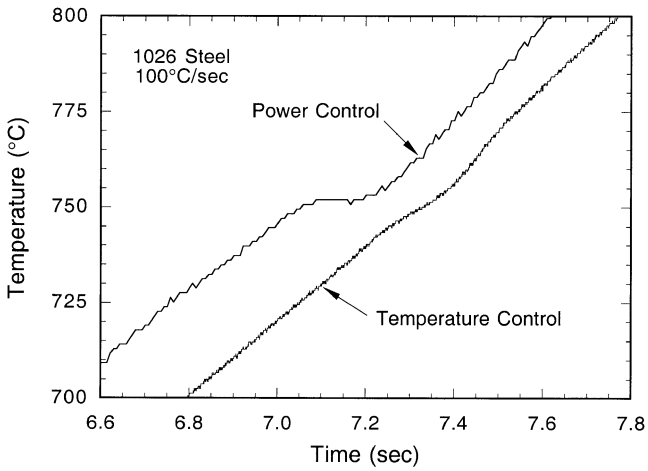

Fig. 8—Comparison of on-heating thermal cycles for controlled-power and controlled-temperature modes for a 100 °C/s heating rate.

Fits to the dilatation data for the controlled-power tests yielded kinetic parameters which were essentially identical

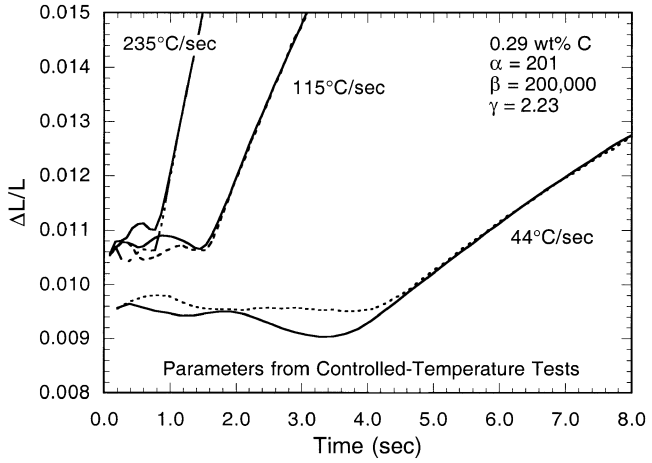

Fig. 9—Comparison of experimental dilatation data (dashed) to prediction (solid) for three different heating rates for the 1026 steel. Controlled-power tests.

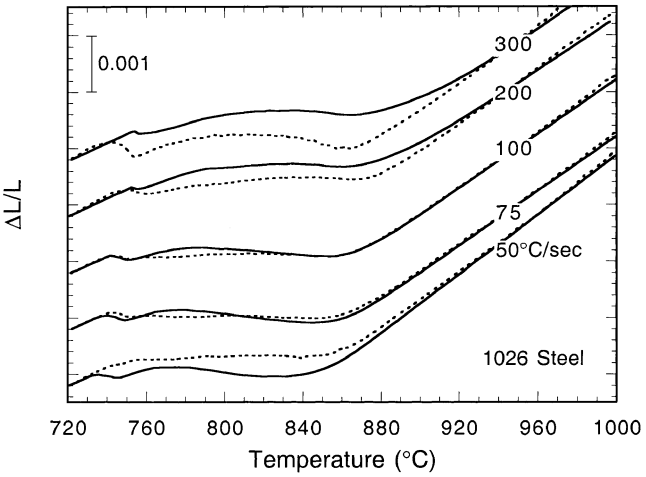

Fig. 10—Comparison of predicted (solid) and measured (dashed) dilatations for heating rates in the range 50 °C/s to 300 °C/s. Predicted curves based on original fitting coefficients of $\alpha = 201$, $\beta = 200{,}000$, and $\gamma = 2.23$. For clarity, the curves are displaced in $\Delta L/L$ (each curve has a value of approximately 0.011 at 720 °C).

to those obtained from the controlled-temperature cycle tests. Hence, the controlled power data are equally well fit using the coefficients derived from the controlled-temperature cycle experiments and *vice versa*. Figure 9 shows the experimental dilatation and model fits for the controlled-power experiments using the coefficients derived from the controlled-temperature cycle tests. The structure and accuracy of the fitted curves are similar to those observed for the controlled-temperature tests (Figure 4). Based on these results, the Avrami/diffusion model captures the differences in transformation rate caused by the differences in thermal cycle for the two control modes. Thus, it is not necessary to modify the kinetic parameters for the 1026 steel at these heating rates. Of course, it is also possible that the current model and experiments are not sensitive enough to detect subtle differences in the kinetic parameters. Based on the rationale that the primary differences between the two control modes would be in the details of nucleation, the effect would be expected to be largest during the transformation of the pearlite constituent. If the nucleation rate of austenite in pearlite is sufficiently high for both thermal cycles, then changes in this rate may not have an appreciable effect on the kinetic fit parameters irrespective of the model used. Also, since the pearlite contributes only approximately one-third volumetrically to the total dilatation, small changes in its decomposition parameters due to the temperature differences between the two modes may not be detectable within the experimental uncertainty. Finally, as mentioned previously, the current model assumes that the cementite and ferrite within the pearlite are consumed proportionally, so that neither phase remains when the pearlite is transformed to austenite. Speich and Szirmae[3] and others[2,6] have shown that cementite (or carbon concentration gradients) can remain in austenite formed from pearlite. Nevertheless, for the particular steel and conditions examined, differences between the transformation rates can be explained solely by differences in the time-temperature path caused by the latent heat and without the need to invoke different kinetic parameters.

As a further test of the model, five additional dilatation measurements were evaluated. These experiments were conducted at heating rates of 50, 75, 100, 200, and 300 °C/s and were compared with predictions based on the kinetic coefficients obtained earlier. Thus, these additional experiments were intended to evaluate the repeatability of the experiments as well as the suitability of the coefficients (α, β, γ) determined previously for interpolation within (75 °C/s) and extrapolation out of (300 °C/s) the bounds for which the coefficients were originally determined (50 °C 200 °C/s). As before, the dilatation curves were self-calibrated to ensure matching in the low- and high-temperature portions of the curves, but again, the required adjustments were less than 1 pct. The results of these trials are shown in Figure 10. For clarity, the curves are displaced from one another along the $\Delta L/L$ ordinate by 0.001 (each curve has a value of approximately 0.001 at 720 °C). Qualitatively, the model generally reproduces the features of the experimental curves, although for the lower heating rates, the predicted local minima are not obvious experimentally. The model generally underpredicts the dilatations for lower heating rates and overpredicts at higher heating rates. Nevertheless, the overall error in the predictions for this range of heating rates is comparatively small. The maximum deviation in $\Delta L/L$ between the estimates and experimental data is 0.0006 (at the second local minima of the 300 °C/s experiment), and this represents an error of approximately 5 pct relative to the total dilatation at this temperature. In addition, there can be variation in the dilatation experiments, as illustrated in Figure 4. Thus, these initial comparisons between the model predictions and experimental measurements indicate that the model accurately reflects the transformation kinetics for this steel. Additional comparisons of the model with direct measurements of fraction transformed, as well as further consideration of the variability of experimental dilatation measurements, will be presented in a future article. However, it should be noted that direct experimental validation of the model is a very difficult problem in itself and has a significant number of uncertainties. For example, one approach is to attempt to quench samples at various times during the reaction and then to examine the microstructure to determine the fraction transformed (*i.e.*, the fraction martensite). Although this ap-

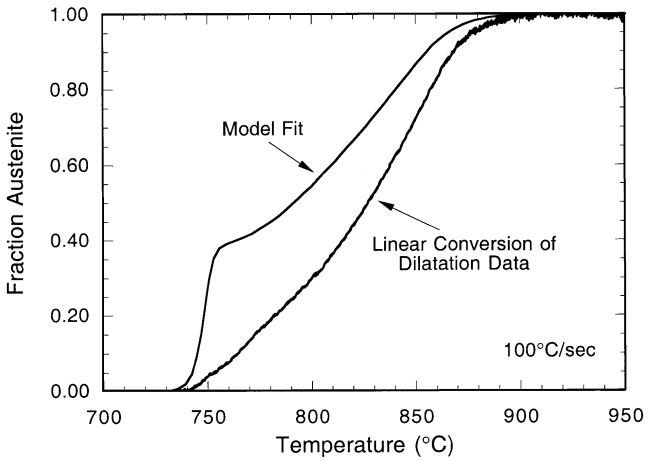

Fig. 11—Comparison of fraction austenite as a function of temperature for the current model and conventional linear conversion of dilatometry data, 100 °C/s.

Table II. Sensitivity of Fit to Various Parameters

Parameter	Symbol	Sensitivity
Fitting parameter	α	3.0
Fitting parameter	β	2.4
Fitting parameter	γ	0.4
Grain size	R_g	0.9
Alloy density	$\underline{\rho}$	0.0
Average carbon content	$\overline{c}$	0.6
Eutectoid temperature	T_e	4.6
Pearlite volume fraction	F_{po}	1.7

proach appears simple in concept, it is extremely difficult in practice for austenitization reactions. First, the timeframe for the reaction is quite rapid, so that interrupting the reaction at a suitable number of different fractions transformed is problematic, and especially difficult during the decomposition of the pearlite constituent. Moreover, the hardenability of partially austenitized structures contributes to additional uncertainties in the experiments. That is, if a sample that contains pearlite or proeutectoid ferrite is quenched, the nucleation event for the formation of these constituents is superceded, so that it is possible (perhaps even probable) that these constuents will grow back to some extent during the quench. This problem becomes even more significant during the latter stages of austenitization when the carbon content of the austenite becomes relatively low (as does the hardenability). Clearly, these difficulties must be resolved and quantified in order to provide a definitive and compelling experimental validation of the kinetic model.

Finally, it is interesting to compare the transformation kinetics as described by the current model with those determined by conventional linear interpolation from dilatometry data. Such a comparison is shown in Figure 11 for a heating rate of 100 °C/s. In the conventional approach, the dilatation of the low- and high-temperature constituents is extrapolated through the transformation temperature range, and then a lever rule method is used to estimate the fraction transformed. In agreement with the observations of Onink *et al.*[14] on the decomposition of austenite into ferrite and cementite, such an approach can lead to significant error in the estimation of the fraction transformed. In fact, for this steel and these heating rates, the transformation of the pearlite and ferrite constituents cannot readily be distinguished by the conventional lever rule approach.

B. *Model Sensitivity*

It is relatively easy to determine the model sensitivity to the various parameters since the fitting procedure yields a numerical value for the summation of the differences between the model and the data. Table II shows the ratio of the fractional change in the fit to the fractional change in each parameter (keeping all other parameters in the table constant). In the table, the sensitivity is defined as

$$S(\Pi) = \left\{ \frac{\Pi}{\sum (d_i - m_i)^2} \right\} \frac{\partial}{\partial \Pi} \left(\left(\sum (d_i - m_i)^2 \right) \right) \quad [21]$$

where S is the sensitivity of parameter Π. The summation, which is over an entire data set, sums the square of the difference between the predicted dilatation (d_i) and the measured dilatation (m_i). Values much greater than 1 imply large sensitivity, and values less than 1 imply low sensitivity.

As can be seen from Table II, the model is most sensitive to the first two fitting parameters (α and β). This is due to the rapid transition of the pearlite to austenite and the sensitivity of the kinetics to the values of these parameters. However, it has been determined that the model is two orders of magnitude less sensitive to changes if the ratio of these parameters is maintained. Thus, it is difficult to determine either of these parameters accurately by this procedure, but their ratio is easily determined.

The self-calibration procedure makes the method insensitive to the density parameter. But, the procedure is sensitive to the volume fraction of pearlite, the eutectoid temperature, and the grain size. However, equally good fits may be obtained using any grain size, for the third fitting parameter (gamma) is simply increased as the grain size increases.

It is stressed here that only the first three parameters in Table II are fitting parameters. Their values are chosen so that the best fit of the experimental data is obtained. The other parameters were obtained from separate measurements. If α or β could be determined from other measurements, then the number of fitting parameters could be reduced. As is typical in multiparameter fits, many parameter combinations yielded almost equally good fits to the data. As described previously, only the ratio between α and β could be accurately determined *via* the fitting procedure, so it is desirable to obtain one of these parameters from a different measurement.

V. CONCLUSIONS

A self-calibration method has been developed to allow interpretation of dilatation data for solid-state phase change reactions. This method may be used when more than one reaction is involved in the transformation. Classical interpretation of such data is especially difficult when the volume change of each reaction is different and both reactions occur simultaneously. In this case, it is impossible to obtain phase fractions by simply using the lever rule on the dila-

tation records. In this study, a model was created that relates the phase transformations to volume changes. By fitting the model to the dilatation data, the transformation kinetics can be inferred. However, experimental and modeling errors make direct comparisons of the data and model output difficult. Therefore, a self-calibration feature was introduced that eliminates many typical errors and allows correct interpretation of the reaction rates. In many cases, the previous procedure is preferred over heat and quench procedures coupled with determination of the phase structure *via* micrographs (since these only determine integral quantities and involve interpretation of the kinetics during the quench). Application of the current procedure requires a minimum amount of material property data.

The model has been applied to dilatation data for a low carbon steel over a range of heating rates. In general, quite good agreement between the model and experiments is realized. The model reproduces the features of the experimental dilatation curves and provides insight into the progress of the transformation that cannot be obtained by simple lever rule–based interpretation of these curves. By fitting to more than one data set, there is greater assurance of the applicability of the model to various heating rates.

ACKNOWLEDGMENTS

The authors acknowledge the efforts of Alice Kilgo for obtaining the pearlite volume fractions and Danny MacCallum for obtaining the dilatation data. The authors also thank Doug Adkins, Michael Hobbs, and Ken Eckelmeyer for their thoughtful reviews of the manuscript. This work was performed at Sandia National Laboratories. Sandia is a multiprogram laboratory operated by Sandia Corporation, a Lockeed Martin Company, for the United States Department of Energy under Contract No. D.E-AC04-94AL85000.

LIST OF SYMBOLS

A_{e3}	upper critical temperature
A	fraction of pearlite transformed to austenite
B	fraction of the ferrite region transformed to austenite
$\bar{c}$	mean carbon content (wt pct)
c	carbon content for a particular phase (wt pct)
d	predicted dilatation
$D(T)$	diffusion coefficient for carbon in austenite (cm^2/s)
F	volume fraction for a particular phase
K	kinetic parameter
L	sample length (m)
M	mass fraction for a particular phase
m	measured dilatation
n	order of reaction
r	radial location in assumed grain geometry (m)
R_1	initial pearlite colony radius (m)
R_g	prior austenite grain radius (m)
$S(\Pi)$	sensitivity fit to changes in parameter Π
t	time (s)
T	temperature (K)
V	volume of unit mass (m^3)
α	kinetic free parameter
β	kinetic free parameter
γ	kinetic free parameter
ΔL	sample length dilatation (m)
Δx	change in distance (m)
Π	input or fitting parameter
ρ	density (g/cm^3)
θ	adjusted time (s)
ω	density multiplier

Subscripts

c	cementite
e	eutectoid temperature
f	ferrite
o	standard temperature
p	pearlite

Superscripts

$\bar{p}$	fraction within pearlite constituent

REFERENCES

1. G.A. Roberts and R.F. Mehl: *Trans. ASM*, 1943, vol. 31, pp. 613-50.
2. E.S. Davenport and E.C. Bain: *Trans. AIME*, 1930, vol. 90, pp. 117-31.
3. G.R. Speich and A. Szirmae: *Trans. AIME*, 1969, vol. 245, pp. 1063-69.
4. G. Molinder: *Acta Metall.*, 1956, vol. 4, pp. 565-71.
5. R.R. Judd and H.W. Paxton: *Trans. AIME*, 1968, vol. 242, pp. 206-15.
6. C.I. Garcia and A.J. DeArdo: *Metall. Trans. A*, 1981, vol. 12A, pp. 521-30.
7. P.A. Wycliffe, G.R. Purdy, and J.D. Embury: *Can. Metall. Q.*, 1981, vol. 20, pp. 339-50.
8. D.F. Watt, L. Coon, M. Bibby, J. Goldak, and C. Henwood: *Acta Metall.*, 1988, vol. 36 (11), pp. 3029-35.
9. T. Akbay, R.C. Reed, and C. Atkinson: *Acta Metall. Mater.*, 1994, vol. 47, pp. 1469-80.
10. C. Atkinson, T. Akbay, and R.C. Reed: *Acta Metall. Mater.*, 1995, vol. 43, pp. 2013-31.
11. C. Atkinson and T. Akbay: *Acta Mater.*, 1996, vol. 44, pp. 2861-68.
12. T. Akbay and C. Atkinson: *J. Mater. Sci.*, 1996, vol. 31, pp. 2221-26.
13. L. Gavard, H.K.D.H. Bhadeshia, D.J.C. MacKay, and S. Suzuki: *Mater. Sci. Technol.*, 1996, vol. 12, pp. 453-63.
14. M. Onink, F.D. Tichelaar, C.M. Brakman, E.J. Mittemeijer, and S. van der Zwaag: *Z. Metallkd.*, 1996, vol. 87, pp. 24-32.
15. A.S. Oddy, J.M.J. McDill, and L. Karlsson: *Can. Met. Q.*, 1996, vol. 35, pp. 275-83.
16. K.W. Andrews: *J. Iron Steel Ins.*, 1965, vol. 203, pp. 721-27.
17. E.A. Brandes: *Smithells Metals Reference Book*, 6th ed., Butterworth and Co., London, 1983, pp. 13-58.
18. J.W. Christian: *The Theory of Phase Transformations in Metals and Alloys, Part I*, Pergamon Press, New York, NY, 1981, pp. 525-48.
19. A. Jacot, M. Swierkosz, J. Rappaz, M. Rappaz, and D. Mari: *Les Ed. Phys.*, 1995, vol. 6, pp. 203-13.
20. W.H. Press, B.P. Flannery, S.A. Teukolsky, and W.T. Vetterling: *Numerical Recipes*, Cambridge University Press, Cambridge, United Kingdom, 1990.
21. C.V. Robino, G.A. Knorovsky, R.C. Dykhuizen, D.O. MacCallum, and B.K. Damkroger: *Proc. 5th Int. Conf. on Trends in Welding Research*, S.A. David, ed., Pine Mountain, GA, 1998, in press.